Supplement of

Mechanistic Insights into I_2O_5 Heterogeneous Hydrolysis and Its Role in Iodine Aerosol Growth in Pristine and Polluted Atmospheres

Xiucong Deng et al.

Correspondence to: An Ning (anning@bit.edu.cn) and Xiuhui Zhang (zhangxiuhui@bit.edu.cn)

Table of Contents

Supplementary Methods

Unbiased BOMD simulations.

Well-tempered metadynamics simulations.

Block average analysis.

Wave function analysis.

Reaction rate constant of the hydrolysis.

Table S1. Reaction rate constants of I_2O_5 hydrolysis mediated by H_2O, I_2O_5, HIO_3, and H_2SO_4.

Figure S1. Temperature (black data) and potential energy (red data) evolution during the Born-Oppenheimer molecular dynamics (BOMD) simulations (for the last 30 ps) of the slab containing 128 water molecules in the constant volume and temperature (*NVT*) ensemble at 300 K. The horizontal lines indicate the mean of temperature (red) and potential energy (black). The small standard deviations of energy (<0.002%) and temperature (<4.7%) indicate that the system has reached a statistical equilibrium.

Figure S2. (a) Snapshot structures of BOMD simulation for methylamine (MA)-mediated I_2O_5 hydrolysis, which illustrate the mechanism for this process. The color coding of different elements is provided below the BOMD snapshot. **(b)** Time-dependent evolution of key bond distances, with arrows showing the transfer and bonding direction of molecular fragments.

Figure S3. (a) Snapshot structures of BOMD simulation for trimethylamine (TMA)-mediated I_2O_5 hydrolysis, which illustrate the mechanism for this process. The color coding of different elements is provided below the BOMD snapshot. **(b)** Time-dependent evolution of key bond distances, with arrows showing the transfer and bonding direction of molecular fragments.

Figure S4. Details of unbiased simulations. Time evolution of I–O bond distances (I1–O and I2–O within I_2O_5) mediated by **(a)** H_2O, **(b)** HIO_3, **(c)** I_2O_5 and **(d)** H_2SO_4. The color-mapped

electron localization function (ELF) for the I_2O_5 is illustrated, indicating no apparent tendency for I_2O_5 to react with interfacial H_2O to form HIO_3.

Figure S5. Collective variable (CV) for the initial metadynamics (MetaD) simulations. This CV was set to investigate potential mechanisms for I_2O_5 hydrolysis.

Figure S6. Collective variable (CV) for the stepwise multi-subphase space metadynamics (SMS-MetaD) simulations. The CV includes all formation (blue) and breaking (red) of bonds during I_2O_5 hydrolysis mediated by **(a)** H_2O, **(b)** I_2O_5, **(c)** HIO_3, and **(d)** H_2SO_4 at the air-water interface. The CV: d_{cv} = d1 + d2 + d3 - d4 - d5 - d6 was set for four SMS-MetaD simulations.

Figure S7. Convergence analysis of the SMS-MetaD simulations for I_2O_5 hydrolysis mediated by H_2O at the air-water interface. **(a)** The free energy profiles. **(b)** Time evolution of CV. **(c)** Time evolution of Gaussian height.

Figure S8. Convergence analysis of the SMS-MetaD simulations for I_2O_5 hydrolysis mediated by I_2O_5 at the air-water interface. **(a)** The free energy profiles. **(b)** Time evolution of CV. **(c)** Time evolution of Gaussian height.

Figure S9. Convergence analysis of the SMS-MetaD simulations for I_2O_5 hydrolysis mediated by HIO_3 at the air-water interface. **(a)** The free energy profiles. **(b)** Time evolution of CV. **(c)** Time evolution of Gaussian height.

Figure S10. Convergence analysis of the SMS-MetaD simulations for I_2O_5 hydrolysis mediated by H_2SO_4 at the air-water interface. **(a)** The free energy profiles. **(b)** Time evolution of CV. **(c)** Time evolution of Gaussian height.

Figure S11. Free energy error as a function of block size within the MetaD simulations of **(a)** H_2O-, **(b)** I_2O_5-, **(c)** HIO_3- and **(d)** H_2SO_4-mediated I_2O_5 hydrolysis. The error increases with the block size but reaches a plateau, where the block size was chosen for block-analysis (red dashed lines).

Figure S12. (a) The products are surrounded by interfacial water, and *x*, *y*, *z* represent the number of water molecules bound by HIO_3, IO_3^-, and MAH^+ ($DMAH^+$ or $TMAH^+$) through hydrogen bond (HB, bond length < 3.5 Å, and bond angle > 150°). The total number for the products that mediated by **(b)** MA, **(c)** dimethylamine (DMA), and **(d)** TMA.

Figure S13. The independent gradient model based on Hirshfeld partition (IGMH) analysis for the products of **(a)** MA-, **(b)** DMA-, and **(c)** TMA-mediated hydrolysis. The blue regions indicate notable attraction, such as hydrogen bonds (HBs) and halogen bonds (XBs). And the green regions indicate van der Waals (vdW) interaction, and the red regions indicate repulsion.

Figure S14. The electrostatic potential (ESP)-mapped molecular vdW surfaces of the interfacial reaction products mediated by **(a)** MA, **(b)** DMA and **(c)** TMA. The red region is the electron-deficient region, and the blue region is the electron-rich region. The yellow sites indicate the points of local maximum electrostatic potential; the cyan sites indicate the points of local minimum electrostatic potential.

Figure S15. Color-mapped ELF for the iodine products (IO_3^- and HIO_3) of I_2O_5 hydrolysis mediated by **(a)** MA, **(b)** DMA, and **(c)** TMA.

Supplementary Methods

Unbiased BOMD simulations.

We first performed unbiased BOMD simulations to check whether the hydrolysis of I_2O_5, mediated by H_2O, HIO_3, I_2O_5, H_2SO_4 and amines (MA, DMA, and TMA; see Figures S2 and S3), can occur rapidly, analyzing the dynamic behavior of the pre-reaction complex. The simulation system has been fully relaxed to reach equilibrium (see Figure S1). Among the studied species, amines quickly promote the hydrolysis (see Figure 6); H_2SO_4-mediated reaction occurs only after 20 ps, indicating that it proceeds more slowly than the amine-mediated reaction; while other chemicals indicate no apparent tendency for I_2O_5 to react with interfacial H_2O to form HIO_3 in the simulations within 50 ps (see Figure S4).

Well-tempered metadynamics simulations.

To investigate the free energy landscape of I_2O_5 hydrolysis at the air-water interface, we performed well-tempered metadynamics (MetaD) simulations (Barducci et al., 2008). Initially, the collective variable (CV) was set to the addition of two I–O bond lengths (see Figure S5), and the sigma widths and heights of Gaussian hills were set to 0.4 Å and 0.9 kcal mol^{-1}, respectively, to explore potential mechanisms. Consequently, we performed MetaD simulations with CV containing all the bonds that are formed or broken during the reaction process (see Figure S6) to describe the reaction and estimate the free energy barrier. Prior to final SMS-MetaD simulations, we identified the upper and lower walls for CV settings through unbiased simulations into the reactant complex (lower wall) and product complex (upper wall). The sigma widths and heights of Gaussian hills were set to 0.1 Å and below 0.1 kcal mol^{-1} (refer to the estimated barrier), respectively, for better accuracy in final simulations. The SMS-MetaD simulations were performed respectively in three separate windows. The Gaussian hills were deposited every 50 steps. All the SMS-MetaD simulations were concluded with convergence analysis (see Figures S7-S10).

Block average analysis.

We reweighted the biased simulations using the metadynamics bias potential obtained at the end of the simulation and assuming a constant bias during the entire course of the simulations (Branduardi et al., 2012). Moreover, block averaging techniques were used to compute the error bars on the estimates for the ensemble average and the free energy obtained from the biased simulations. The error increases with the block size but reaches a plateau, where the block size was chosen for block-analysis (see Figure S11). The estimated error bars are exhibited as the pink regions in the free energy profiles.

Wave function analysis.

All wave function analysis for products of I_2O_5 hydrolysis was performed using Multiwfn 3.7 code (Lu and Chen, 2012). All the wave function data was calculated at the same level of theory as the unbiased BOMD simulations by CP2K 2022 program (Kühne et al., 2020). We calculated the number of hydrogen bonds (HBs, bond length < 3.5 Å, and bond angle > 150°) between the products and interfacial water (Figure S12). For further insight into the intermolecular interactions, the independent gradient model based on Hirshfeld partition (IGMH) analysis (Lu and Chen, 2022a, b) was performed, replacing the free-state atomic densities involved in the IGM method (Lefebvre et al., 2017) with the atomic densities derived by Hirshfeld partition of actual molecular electron density (Figure S13). Specifically, the sign(λ_2)ρ values are mapped on the isosurfaces by different colors, where the ρ is electron density and sign(λ_2) denotes the sign of the second largest eigenvalue of Hessian matrix of the ρ. The ρ is usually positively correlated to interaction strength and sign(λ_2) is a normal evidence for distinguishing whether the interaction is attractive or repulsive (Johnson et al., 2010; Lu and Chen, 2012). Moreover, we performed ESP analysis to identify the vacant sites of the products (Figure S14). ELF calculations were performed to identify whether a chemical reaction occurs, specifically by identifying the formation of new chemical bonds.

Reaction rate constant of the hydrolysis.

In this study, the reaction rate constant k is obtained based on transition state theory (TST). The reaction rate constant is given by the following formula:

$$k^{\mathrm{TST}} = \sigma \frac{k_{\mathrm{B}}T}{h} e^{-\Delta G^{0,\neq}/(RT)}$$

where σ is the reaction path degeneracy, k_{B} is the Boltzmann constant, T is the absolute temperature (300 K), h is the Planck constant, R is the molar gas constant, and $\Delta G^{0,\neq}$ is the Gibbs free energy change from reactants to the transition state, i.e., the reaction barrier. The k^{TST} for I_2O_5 hydrolysis is shown in table S1.

Table S1. Reaction rate constants of I_2O_5 hydrolysis mediated by H_2O, I_2O_5, HIO_3, and H_2SO_4.

	$\Delta G^{0,\neq}$ (error range)/kcal mol^{-1}	k^{TST}/M^{-1} s^{-1}	error range of k^{TST}/M^{-1} s^{-1}
H_2O	9.4 ± 0.10	8.81×10^{5}	7.45×10^{5}-1.04×10^{6}
I_2O_5	3.5 ± 0.15	1.76×10^{10}	1.37×10^{10}-2.26×10^{10}
HIO_3	4.3 ± 0.25	4.59×10^{9}	3.02×10^{9}-6.99×10^{9}
H_2SO_4	1.3 ± 0.10	7.06×10^{11}	5.97×10^{11}-8.34×10^{11}

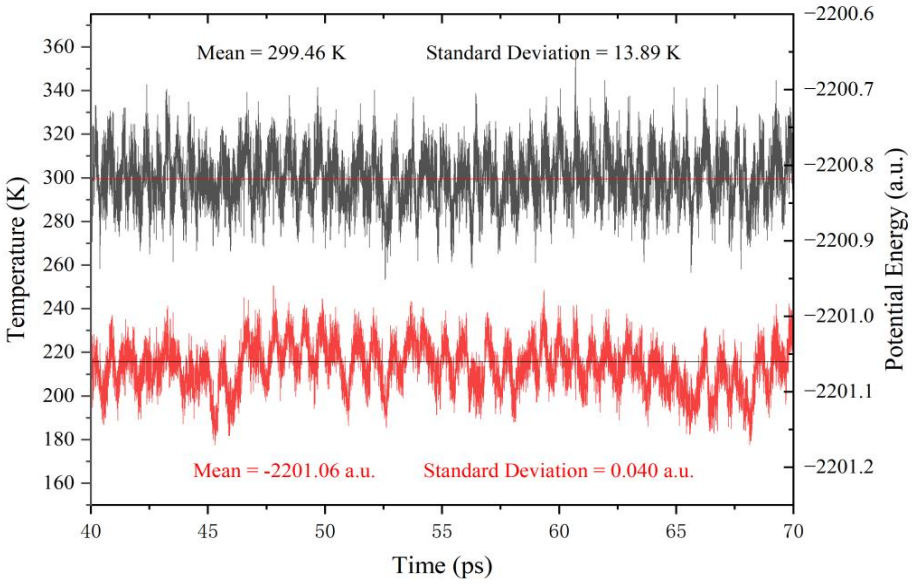

Figure S1. Temperature (black data) and potential energy (red data) evolution during the Born-Oppenheimer molecular dynamics (BOMD) simulations (for the last 30 ps) of the slab containing 128 water molecules in the constant volume and temperature (*NVT*) ensemble at 300 K. The horizontal lines indicate the mean of temperature (red) and potential energy (black). The small standard deviations of energy (<0.002%) and temperature (<4.7%) indicate that the system has reached a statistical equilibrium.

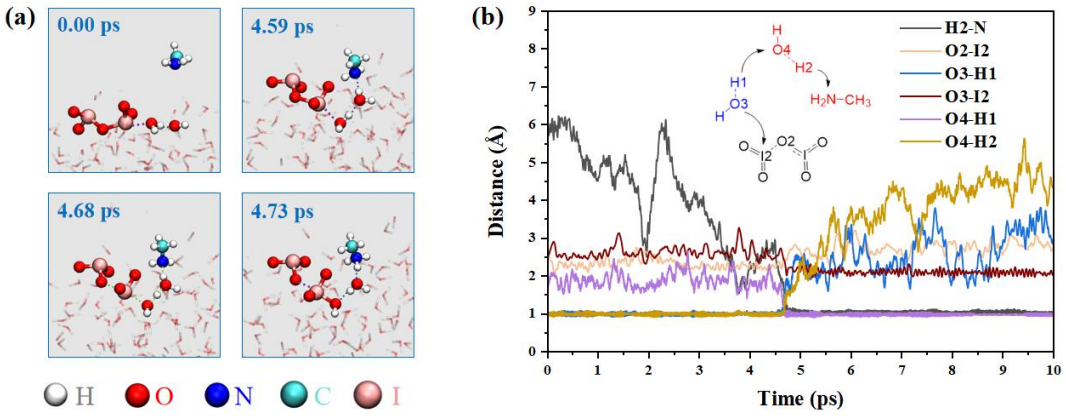

Figure S2. (a) Snapshot structures of BOMD simulation for methylamine (MA)-mediated I_2O_5 hydrolysis, which illustrate the mechanism for this process. The color coding of different elements is provided below the BOMD snapshot. **(b)** Time-dependent evolution of key bond distances, with arrows showing the transfer and bonding direction of molecular fragments.

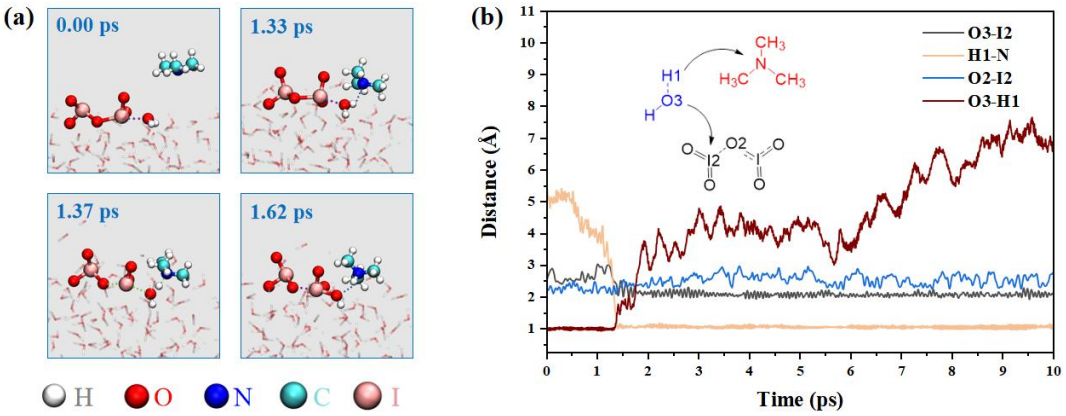

Figure S3. (a) Snapshot structures of BOMD simulation for trimethylamine (TMA)-mediated I_2O_5 hydrolysis, which illustrate the mechanism for this process. The color coding of different elements is provided below the BOMD snapshot. **(b)** Time-dependent evolution of key bond distances, with arrows showing the transfer and bonding direction of molecular fragments.

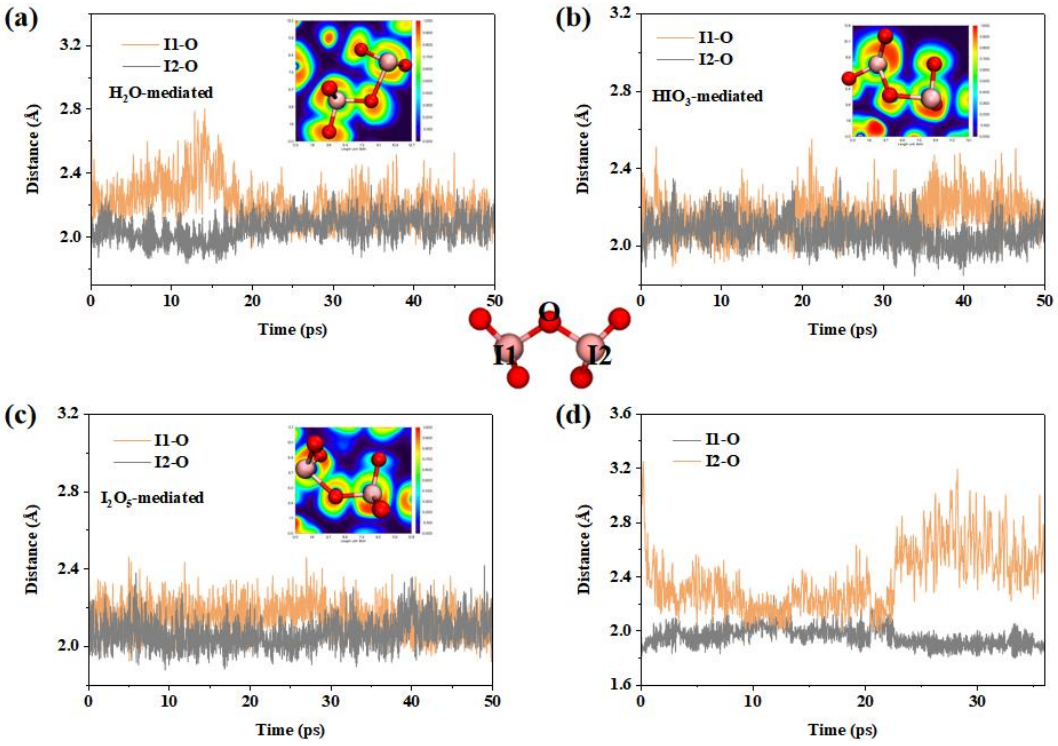

Figure S4. Details of unbiased simulations. Time evolution of I–O bond distances (I1–O and I2–O within I_2O_5) mediated by **(a)** H_2O, **(b)** HIO_3, **(c)** I_2O_5 and **(d)** H_2SO_4. The color-mapped electron localization function (ELF) for the I_2O_5 is illustrated, indicating no apparent tendency for I_2O_5 to react with interfacial H_2O to form HIO_3.

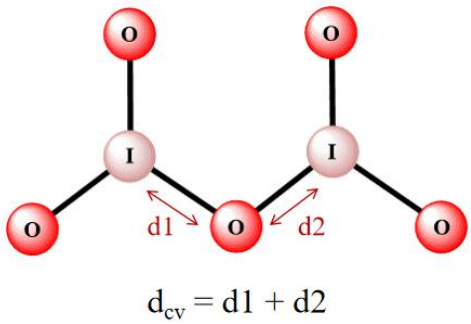

Figure S5. Collective variable (CV) for the initial metadynamics (MetaD) simulations. This CV was set to investigate potential mechanisms for I_2O_5 hydrolysis.

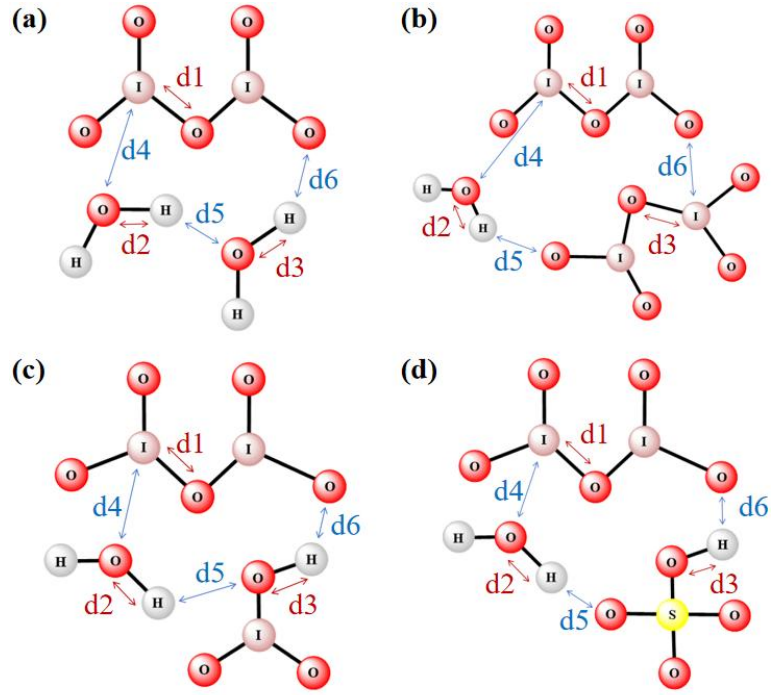

$$d_{cv} = d1 + d2 + d3 - d4 - d5 - d6$$

Figure S6. Collective variable (CV) for the stepwise multi-subphase space metadynamics (SMS-MetaD) simulations. The CV includes all formation (blue) and breaking (red) of bonds during I_2O_5 hydrolysis mediated by **(a)** H_2O, **(b)** I_2O_5, **(c)** HIO_3, and **(d)** H_2SO_4 at the air-water interface. The CV: $d_{cv} = d1 + d2 + d3 - d4 - d5 - d6$ was set for four SMS-MetaD simulations.

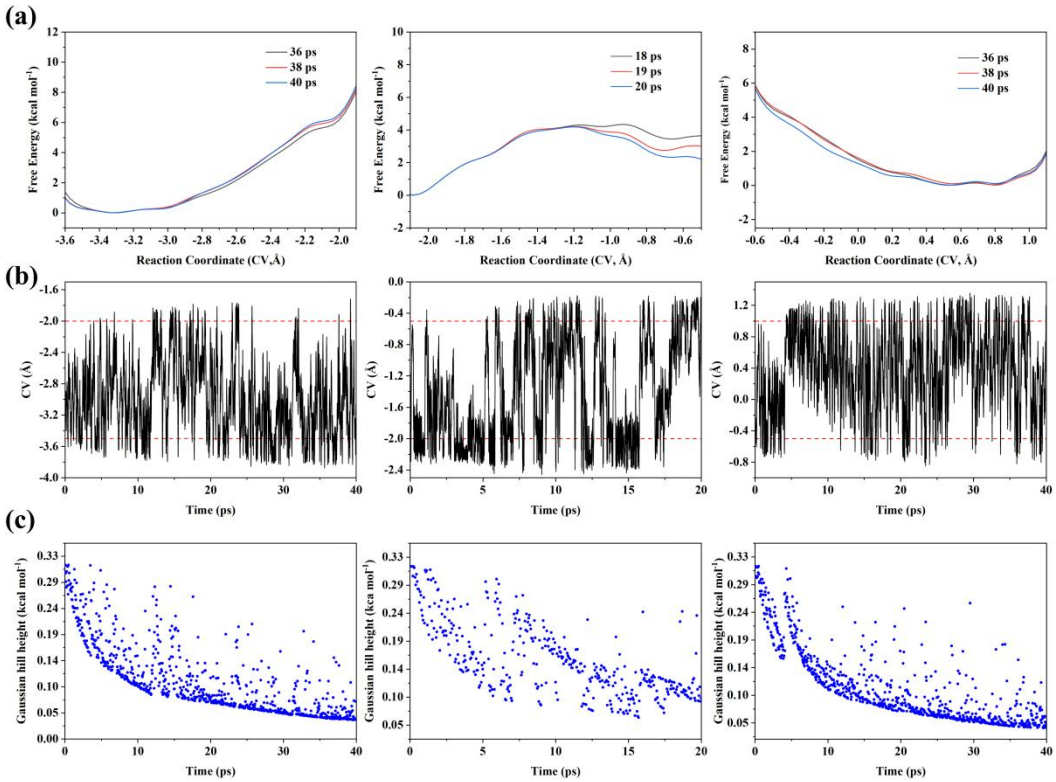

Figure S7. Convergence analysis of the SMS-MetaD simulations for I_2O_5 hydrolysis mediated by H_2O at the air-water interface. **(a)** The free energy profiles. **(b)** Time evolution of CV. **(c)** Time evolution of Gaussian height.

The SMS-MetaD simulations were carried out in three separate windows. Minor variation in the free energy profiles during the final few picoseconds indicates convergence; the CV fluctuates over whole restrained scale (the red dashed lines indicate the upper and lower limits of the windows), indicating the convergence of the CV. The Gaussian height is decreasing to a minimum. Notably, in the beginning the value of the Gaussian height is higher than the initial height we set due to the pre-factor. The free energy profiles and time evolution of CV indicate the convergence reached. The decreasing Gaussian height indicates a conclusion for simulations. The similar results are observed in the following Figures S8-S10, which involve the reactions mediated by I_2O_5, HIO_3 and H_2SO_4.

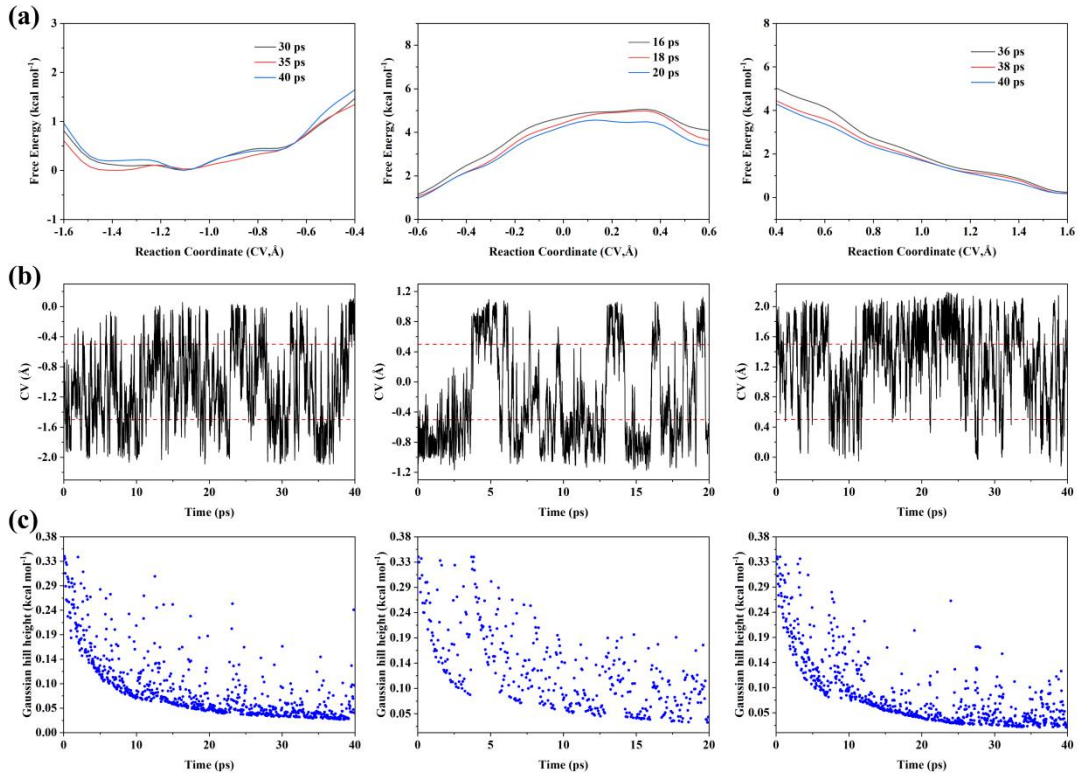

Figure S8. Convergence analysis of the SMS-MetaD simulations for I_2O_5 hydrolysis mediated by I_2O_5 at the air-water interface. **(a)** The free energy profiles. **(b)** Time evolution of CV. **(c)** Time evolution of Gaussian height.

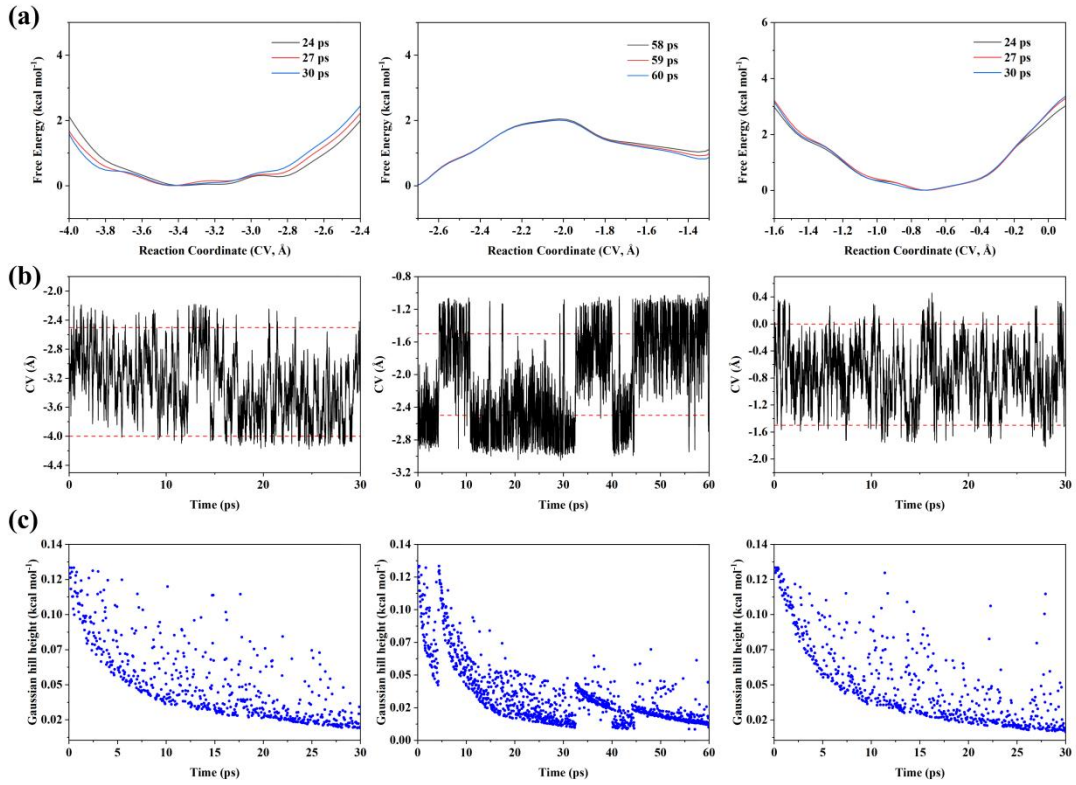

Figure S9. Convergence analysis of the SMS-MetaD simulations for I_2O_5 hydrolysis mediated by HIO_3 at the air-water interface. **(a)** The free energy profiles. **(b)** Time evolution of CV. **(c)** Time evolution of Gaussian height.

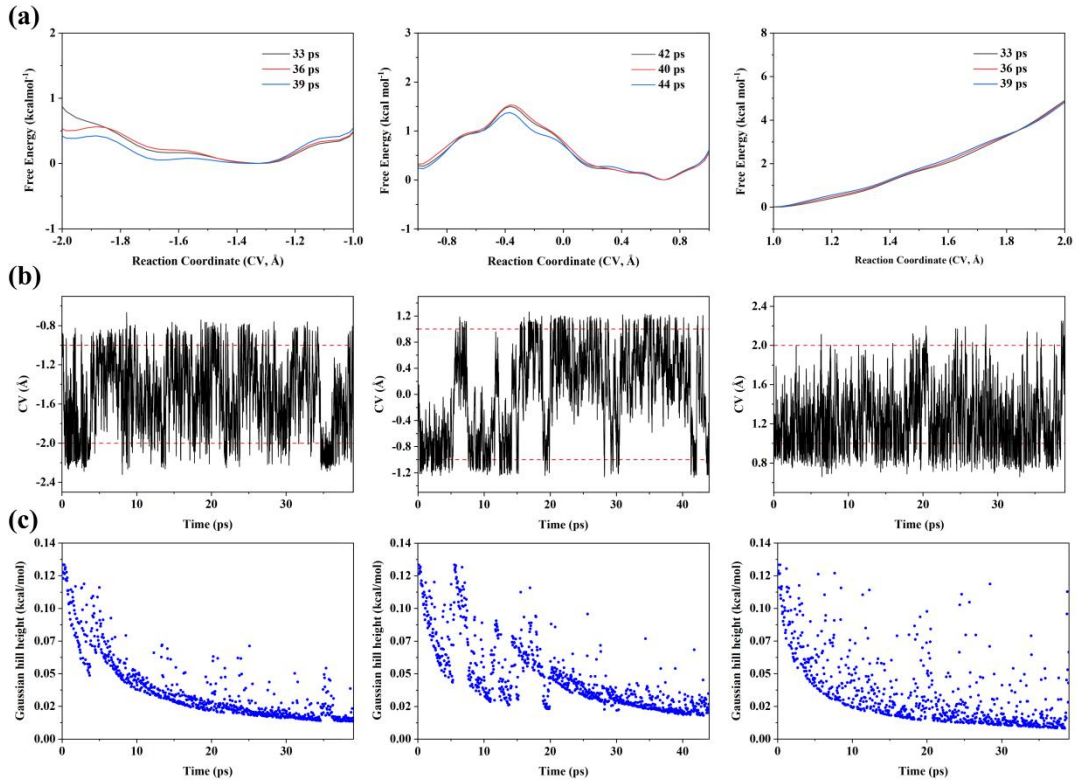

Figure S10. Convergence analysis of the SMS-MetaD simulations for I_2O_5 hydrolysis mediated by H_2SO_4 at the air-water interface. **(a)** The free energy profiles. **(b)** Time evolution of CV. **(c)** Time evolution of Gaussian height.

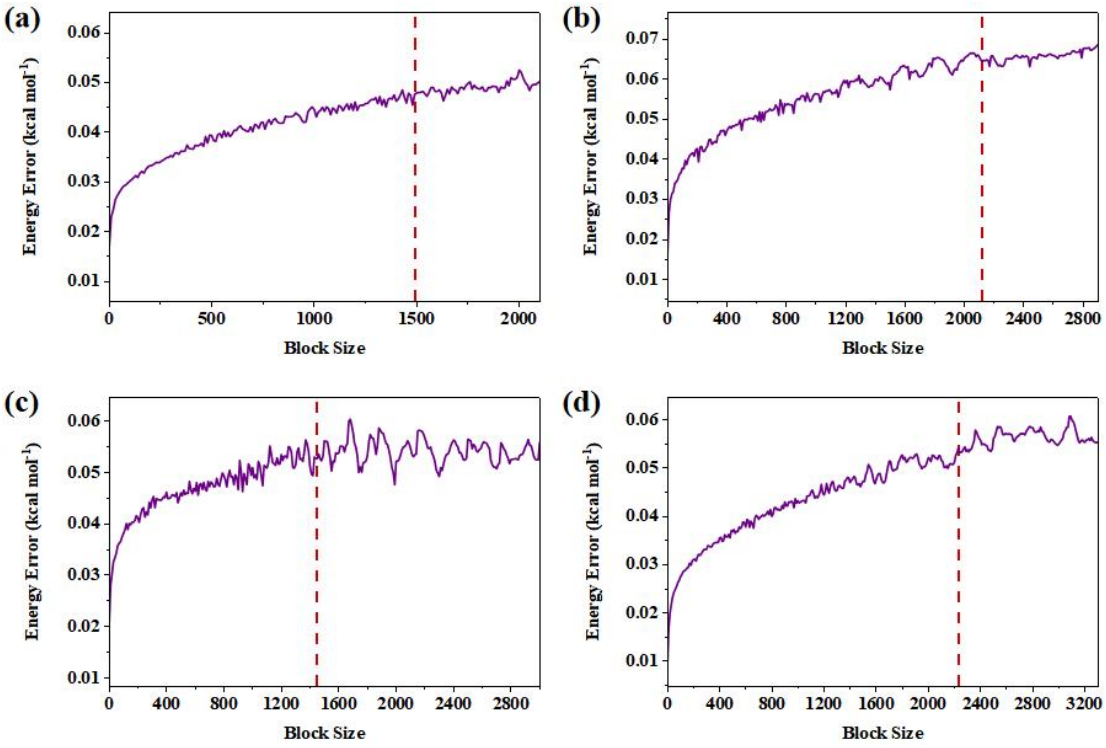

Figure S11. Free energy error as a function of block size within the MetaD simulations of **(a)** H_2O-, **(b)** I_2O_5-, **(c)** HIO_3- and **(d)** H_2SO_4-mediated I_2O_5 hydrolysis. The error increases with the block size but reaches a plateau, where the block size was chosen for block-analysis (red dashed lines).

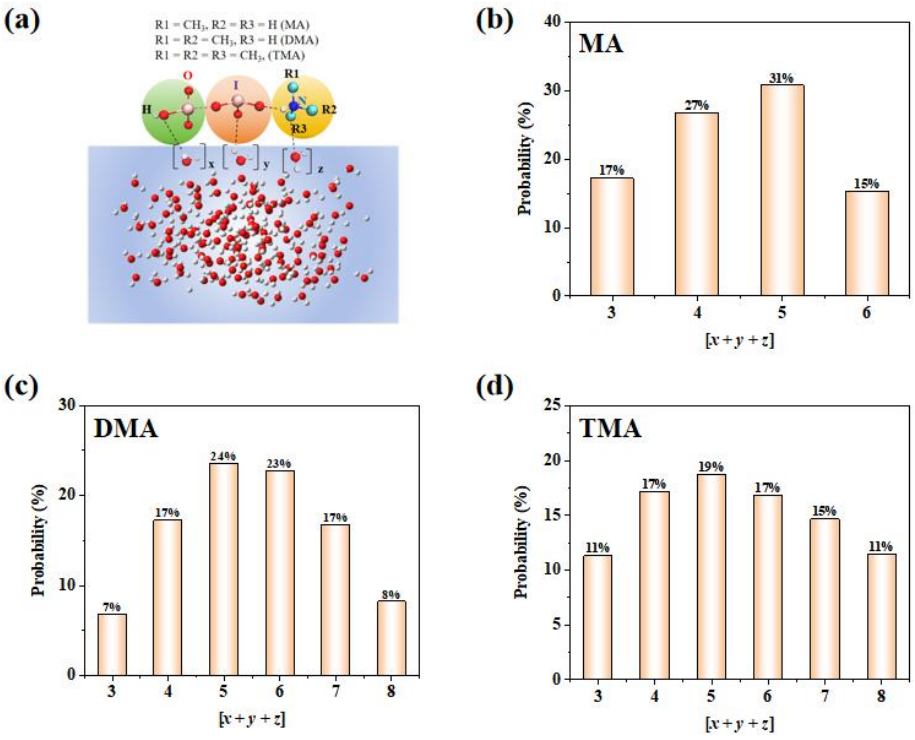

Figure S12. (a) The products are surrounded by interfacial water, and *x*, *y*, *z* represent the number of water molecules bound by HIO_3, IO_3^-, and MAH^+ ($DMAH^+$ or $TMAH^+$) through hydrogen bond (HB, bond length < 3.5 Å, and bond angle > 150°). The total number for the products that mediated by **(b)** MA, **(c)** dimethylamine (DMA), and **(d)** TMA.

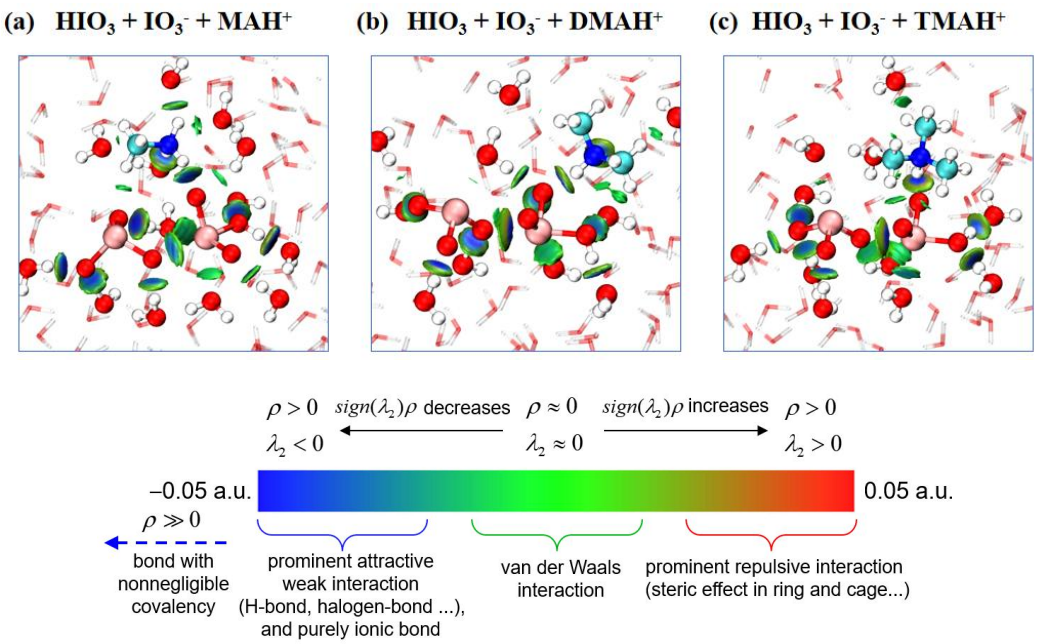

Figure S13. The independent gradient model based on Hirshfeld partition (IGMH) analysis for the products of **(a)** MA-, **(b)** DMA-, and **(c)** TMA-mediated hydrolysis. The blue regions indicate notable attraction, such as hydrogen bonds (HBs) and halogen bonds (XBs). And the green regions indicate van der Waals (vdW) interaction, and the red regions indicate repulsion.

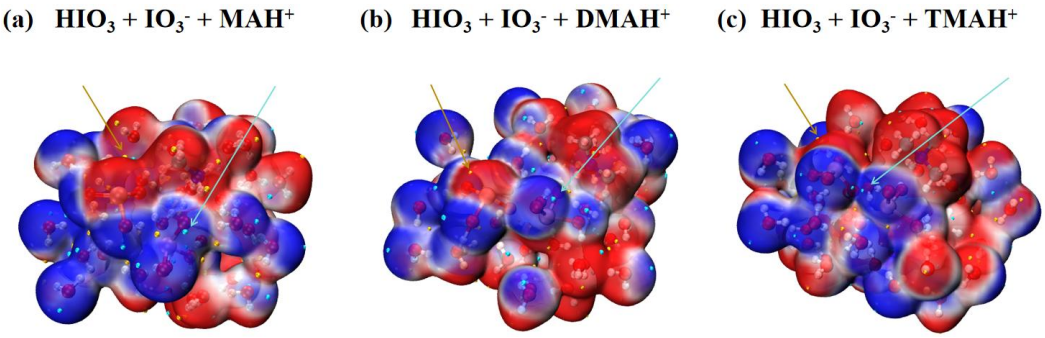

Figure S14. The electrostatic potential (ESP)-mapped molecular vdW surfaces of the interfacial reaction products mediated by **(a)** MA, **(b)** DMA and **(c)** TMA. The red region is the electron-deficient region, and the blue region is the electron-rich region. The yellow sites indicate the points of local maximum electrostatic potential; the cyan sites indicate the points of local minimum electrostatic potential.

For more distinct visualization, only the electrostatic potential (ESP) analysis of the products and surrounding water molecules are shown in Figure S14. The points of local maximum electrostatic potential (near the I within IO_3^- and HIO_3) are the expected unoccupied donor sites for XB and the points of local minimum electrostatic potential (near the O within IO_3^- and HIO_3) are the expected unoccupied acceptor sites for HB and XB. The unoccupied sites potentially further uptake gaseous species, thereby promoting aerosol growth.

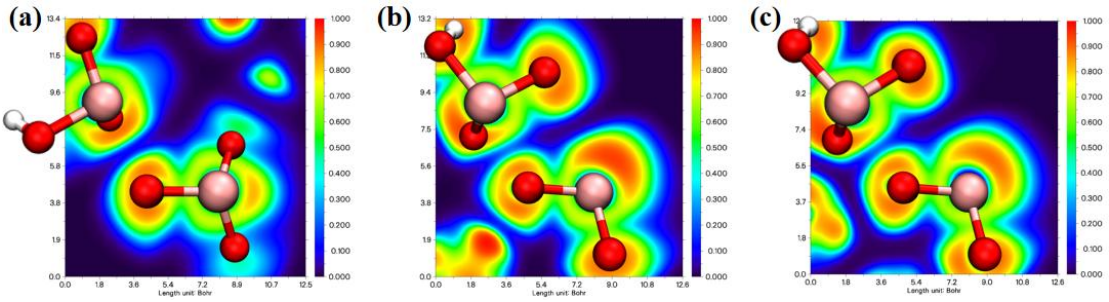

Figure S15. Color-mapped ELF for the iodine products (IO_3^- and HIO_3) of I_2O_5 hydrolysis mediated by **(a)** MA, **(b)** DMA and **(c)** TMA.

Supplementary Reference

Barducci, A., Bussi, G., and Parrinello, M.: Well-Tempered Metadynamics: A Smoothly Converging and Tunable Free-Energy Method, Phys. Rev. Lett., 100, 020603, https://doi.org/10.1103/PhysRevLett.100.020603, 2008.

Branduardi, D., Bussi, G., and Parrinello, M.: Metadynamics with Adaptive Gaussians, J. Chem. Theory Comput., 8, 2247–2254, https://doi.org/10.1021/ct3002464, 2012.

Johnson, E. R., Keinan, S., Mori-Sánchez, P., Contreras-García, J., Cohen, A. J., and Yang, W.: Revealing Noncovalent Interactions, J. Am. Chem. Soc., 132, 6498–6506, https://doi.org/10.1021/ja100936w, 2010.

Kühne, T. D., Iannuzzi, M., Del Ben, M., Rybkin, V. V., Seewald, P., Stein, F., Laino, T., Khaliullin, R. Z., Schütt, O., Schiffmann, F., Golze, D., Wilhelm, J., Chulkov, S., Bani-Hashemian, M. H., Weber, V., Borštnik, U., Taillefumier, M., Jakobovits, A. S., Lazzaro, A., Pabst, H., Müller, T., Schade, R., Guidon, M., Andermatt, S., Holmberg, N., Schenter, G. K., Hehn, A., Bussy, A., Belleflamme, F., Tabacchi, G., Glöß, A., Lass, M., Bethune, I., Mundy, C. J., Plessl, C., Watkins, M., VandeVondele, J., Krack, M., and Hutter, J.: CP2K: An electronic structure and molecular dynamics software package - Quickstep: Efficient and accurate electronic structure calculations, J. Chem. Phys., 152, 194103, https://doi.org/10.1063/5.0007045, 2020.

Lefebvre, C., Rubez, G., Khartabil, H., Boisson, J.-C., Contreras-García, J., and Hénon, E.: Accurately extracting the signature of intermolecular interactions present in the NCI plot of the reduced density gradient versus electron density, Phys. Chem. Chem. Phys., 19, 17928–17936, https://doi.org/10.1039/C7CP02110K, 2017.

Lu, T. and Chen, F.: Multiwfn: A multifunctional wavefunction analyzer, J. Comput. Chem., 33, 580–592, https://doi.org/10.1002/jcc.22885, 2012.

Lu, T. and Chen, Q.: Independent gradient model based on Hirshfeld partition: A new method for visual study of interactions in chemical systems, J. Comput. Chem., 43, 539–555, https://doi.org/10.1002/jcc.26812, 2022a.

Lu, T. and Chen, Q.: Erratum to “Independent gradient model based on Hirshfeld partition: A new method for visual study of interactions in chemical systems,” https://doi.org/10.26434/chemrxiv-2022-g1m34, 26 October 2022b.